Sustainable Water Resources Management (2024) 10:161
https://doi.org/10.1007/s40899-024-01139-7

ORIGINAL ARTICLE

Geochemical and isotopic characterization of the thermal waters in the Cuenca Alta Del Rio Laja basin, Guanajuato, Mexico

Lucía Magali Ramírez-González[1] · María Jesús Puy-Alquiza[2] · Yanmei Li[2] · Jesús Horacio Hernández-Anguiano[2] · Raúl Miranda-Avilés[2] · Rosa María Prol-Ledesma[3]

Received: 28 February 2024 / Accepted: 20 July 2024

Abstract
The thermal waters in the Cuenca Alta del Río Laja basin supply water for agricultural use, human consumption, and spas. The study included 25 groundwater samples from wells in the central part of the basin; 14 of those samples are considered thermal water, as their temperatures are higher than 29ºC. The thermal waters are sodium-bicarbonate type with geochemical signatures similar to those of non-thermal waters, showing a regional flow system evolution. Isotopic composition ($\delta^{18}O$ and δD) of thermal water indicates meteoric origin without a significant $\delta^{18}O$ enrichment. Cl/B ratios may indicate two thermal aquifers. Vertical flow is mostly caused by pumping, and the permeability seems to be controlled by the regional fault system. Chalcedony and multicomponent geothermometry suggest that at depth, the temperature may reach values between 84 and 126ºC. The estimated temperature allows utilization of the thermal water direct uses that include aquaculture, food processing and fruit, vegetable and grains drying.

Keywords Groundwater · Low-enthalpy · Direct uses · Geochemistry · Stable isotopes

Introduction

Thermal waters in the Cuenca Alta del Río Laja (CARL - Upper Basin of the Laja River), have been used since pre-Hispanic times by the local population for health purposes (Salamanca-Corredor and Puy-Alquiza 2017). The intense extraction of groundwater for agricultural and urban use has caused the disappearance of many thermal-springs that were reported in historical records (Navarro de León et al. 2005). Additionally, thermal water is extracted to be used in spas located in the San Miguel de Allende-Atotonilco touristic corridor. Most groundwater wells (90%), supply the agricultural sector (CONAGUA 2020 a, b). The two aquifers in the center of the basin are administrated by CONAGUA (Water Administration Governmental Commission – COmisión Nacional del AGUA in Spanish): the Cuenca Alta del Río Laja aquifer on the west, and the Laguna Seca aquifer on the east; both aquifers have been over-exploited and present a negative value for groundwater availability: -62.5 hm^3/year, and −31.8 hm^3/yr respectively (CONAGUA 2020 a, b).

Thermal waters are defined as a general name for any discharge of deep-seated, pure, or mineralized water whose temperature is consistently higher than the local mean annual temperature of the atmosphere (Panichi and La Ruffa 2009). In this study, groundwater with higher temperature than 29ºC is referred as thermal-water according to the Schoeller classification in Custodio and Llamas (1983), that defines thermal-waters as those with $t > t_m + 4ºC$; where t is the water temperature, and t_m the annual mean temperature, this last parameter is ~ 25ºC for the center of the basin and the maximum recorded for the whole CARL (Servicio Metereológico Nacional 2023).

In the study area there is no evidence of a high temperature geothermal system; therefore, the possibilities of direct uses were evaluated. At low to intermediate temperature

✉ Lucía Magali Ramírez-González
lmramirezgonzalez@ugto.mx

1 Doctoral Program of Water Science and Technology, Engineering Division, Universidad de Guanajuato, Guanajuato, Guanajuato 36000, Mexico

2 Department of Mining, Metallurgy and Geology Engineering, Universidad de Guanajuato, Guanajuato, Guanajuato 36020, Mexico

3 Institute of Geophysics, Universidad Nacional Autónoma de México, Mexico City 04510, Mexico

Published online: 06 August 2024

(< 150ºC), geothermal energy can be utilized in the agriculture and agro-industry sectors, for example in aquaculture, mushroom culture, fruit wine making, and dehydration of agricultural products (Nguyen et al. 2015; Popovski and Vasilevska 2004) as shown in Fig. 1.

Previous geochemical studies carried out in the CARL were focused in understanding the high arsenic and fluoride concentrations in the basin, because in most of the wells, their concentration exceeds the guideline values of 10 µg/L for arsenic, and 1.5 mg/L for fluoride according to the Mexican and International regulations for drinking water (NOM-127-SSA1-2021; World Health Organization 2022). The enrichment of groundwater in those components had been explained as a result of mixing of thermal waters with groundwater due to the intense groundwater exploitation (Ortega-Guerrero 2009). Knappett et al. (2020) and Piña-González et al. (2022), observed that faults may have local importance in the rising of geothermal waters upward flow that favored mixing with shallow aquifers. Therefore, in this study, the center of the basin was selected as the study area because it contains the deepest water-table depths (INEGI 2019; Li et al. 2020), and it is traversed by the N-S Taxco-San Miguel de Allende Fault System that acts as a cortical limit and may represent a channel for the thermal water upward flow (Alaniz-Álvarez et al. 2001, 2002).

This study provides new geochemical and isotopic information of thermal waters from the central part of the CARL. The data processing includes the water type distribution and isotopic signatures, temperature estimation with geothermometers, and chloride and boron distribution analysis. These results are used to describe the reservoir characteristics and the processes involved during the lateral and vertical flow, and compare the results with those available for groundwater. It is expected that the results of this work will improve the hydric resource exploitation conditions in the CARL and diversify the utilization of thermal water.

Study area

Hydrogeologic settings

The Cuenca Alta del Río Laja basin, also unofficially called, Independence basin, is located in central Mexico, in the north of Guanajuato state (Fig. 2). The climate of the CARL is semi-arid. The average precipitation in summer is 3.38 mm, the mean annual temperature in the whole basin is 17 °C, the average annual minimum temperature is 8.8 °C and the maximum is 25 °C (Servicio Metereológico Nacional, 2023); the lowest temperatures are recorded in higher elevations, and the highest temperatures in the center of the basin.

The Río Laja is the main river running from the ranges of Santa Barbara, Sierra de Guanajuato, and El Cubo in the northwest (maximum elevations of 2851, 2952 and 2853 m.a.s.l. respectively), towards the Ignacio Allende dam in the south (1837 m.a.s.l.). Intermittent streams have been used mainly to meet the demands of the agricultural sector with hydraulic structures such as dams (INEGI 1998). The CONAGUA has divided the CARL in five administrative aquifers (CONAGUA 2020a, b, c, d, e). The study area, in the center of the basin, comprises the aquifer Cuenca Alta del Río Laja in the west, and the Laguna Seca aquifer in the east (Fig. 2). The Cuenca Alta del Río Laja is a granular aquifer hosted by continental sediments and pyroclastic deposits, while the Laguna Seca aquifer is also granular but hosted mainly by pyroclastic deposits and fractured volcanic rocks; both have been classified as

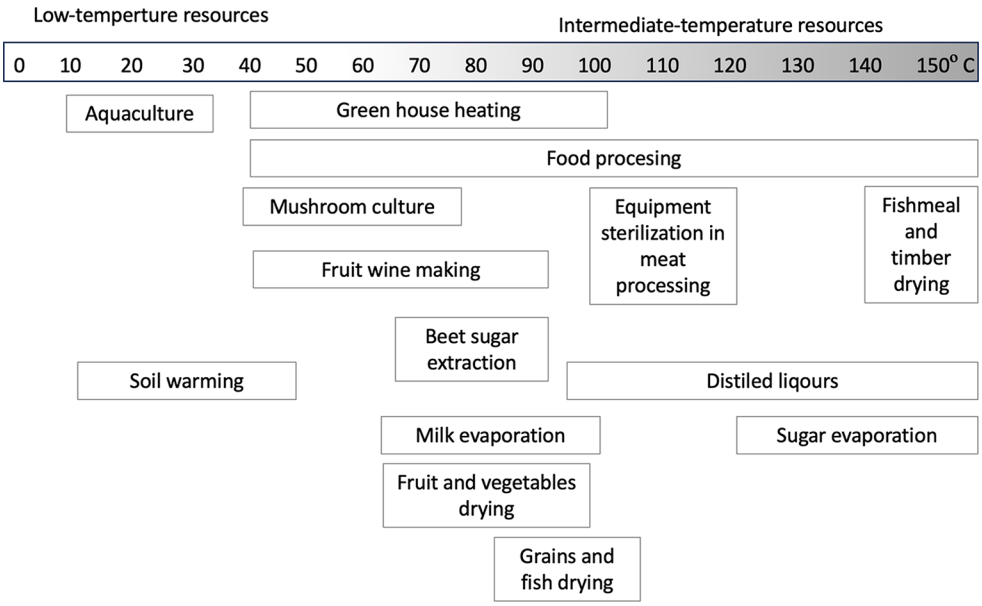

Fig. 1 Lindal diagram (for temperature < 150ºC) of potential uses of geothermal energy in the agriculture and agro-industry sectors. Modified from Nguyen et al. (2015)

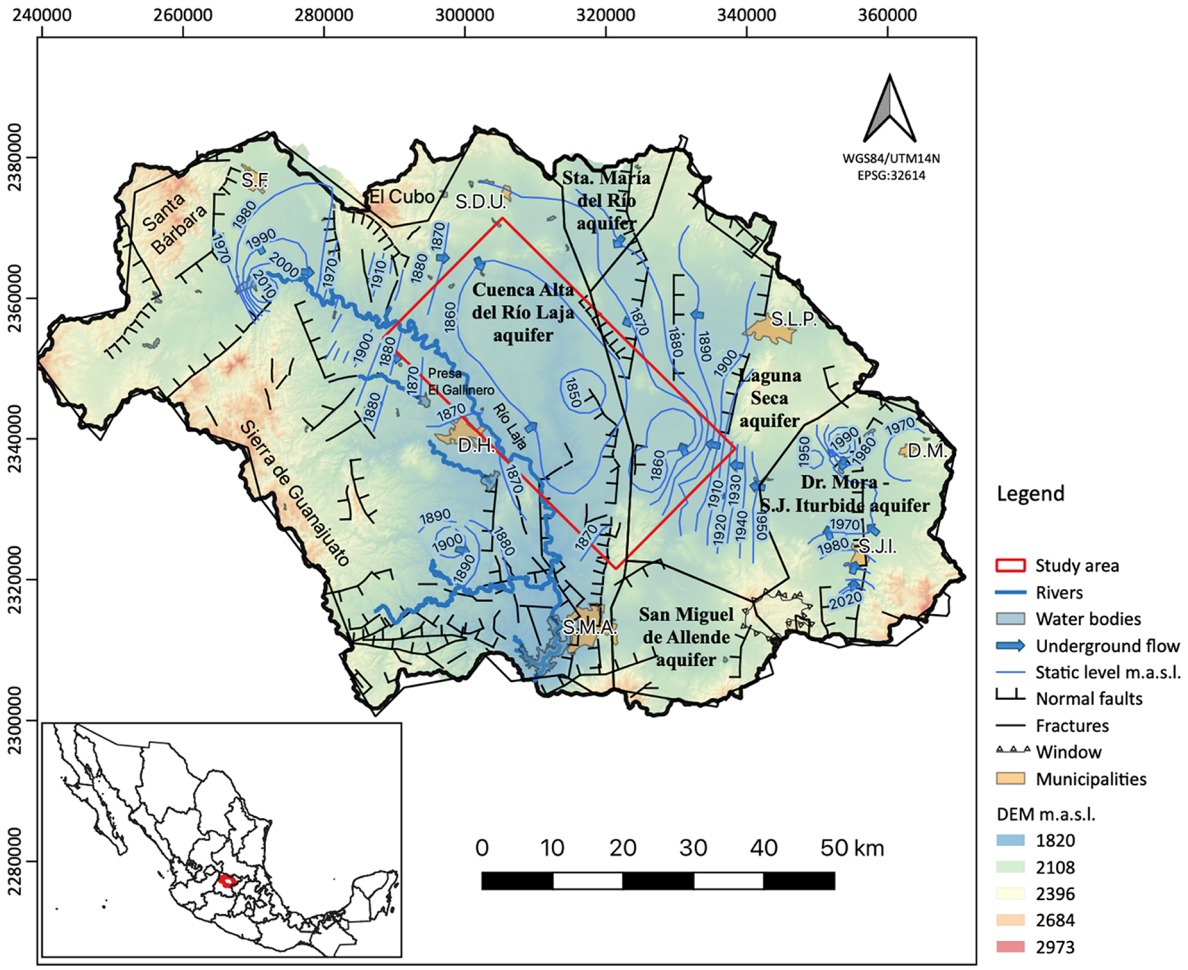

Fig. 2 The Cuenca Alta del Río Laja basin. Underground flow and static level values taken from INEGI (2019). DEM from INEGI (2021). D.H.- Dolores Hidalgo; S.F.- San Felipe; S.D.U.- San Diego de la Unión; S.L.P.- San Luis de la Paz; D.M.- Doctor Mora; S.J.I.- San José Iturbide; S.M.A.- San Miguel de Allende. Faults and fractures from SGM (1997,1999), Alaniz-Álvarez et al. (2002, 2005), and Del Pilar-Martínez et al. (2020)

free aquifers (CONAGUA 2020a, b). However, at the center of the basin they become semiconfined (Mahlknecht et al. 2004). The underground flow has a preferential direction towards the center of the basin (Fig. 2), and the lowest water-table levels are related to cones of depression (INEGI 2019). Both aquifers are exploited by the agricultural sector at 90% of their capacity, and according to CONAGUA (2020a, b), the annual volumes of natural discharge and groundwater extraction exceed the annual recharge volume; therefore, they have a negative value for groundwater availability of -62.5 hm^3/year for the Cuenca Alta del Río Laja aquifer, and −31.8 hm^3/yr for the Laguna Seca aquifer. Li et al. (2020) calculated a water-table velocity of -0.43 m/year for the Cuenca Alta del Río Laja aquifer during the period 2008–2015, and concluded that if the observed drawdown rate continues, by the year 2035, 45% of the aquifer upper area will have a water-table depth greater than 120 m below surface, 24% below 150 m, and in 5% could exceed the 180 m.

The average recharge rate in the basin is 25 mm per year, with minimum values in the northern plains of the basin (10 mm/year in San Diego de la Unión) and maximum values in mountainous areas where local infiltration can be equivalent to the precipitation rate (> 800 mm/year in the Sierra de Guanajuato); and recharge conditions have not changed over the last 10,000–13,000 years (Mahlknecht et al. 2004).

Geologic settings

The simplified CARL geology is presented in Fig. 3. The study area is situated in the southeast limit of the Sierra Madre Occidental volcanic province, and the westernmost Mexican Fold-Thrust Belt (Nieto-Samaniego et al. 1999; Martini et al. 2016; Fitz-Díaz et al. 2018); in the south of

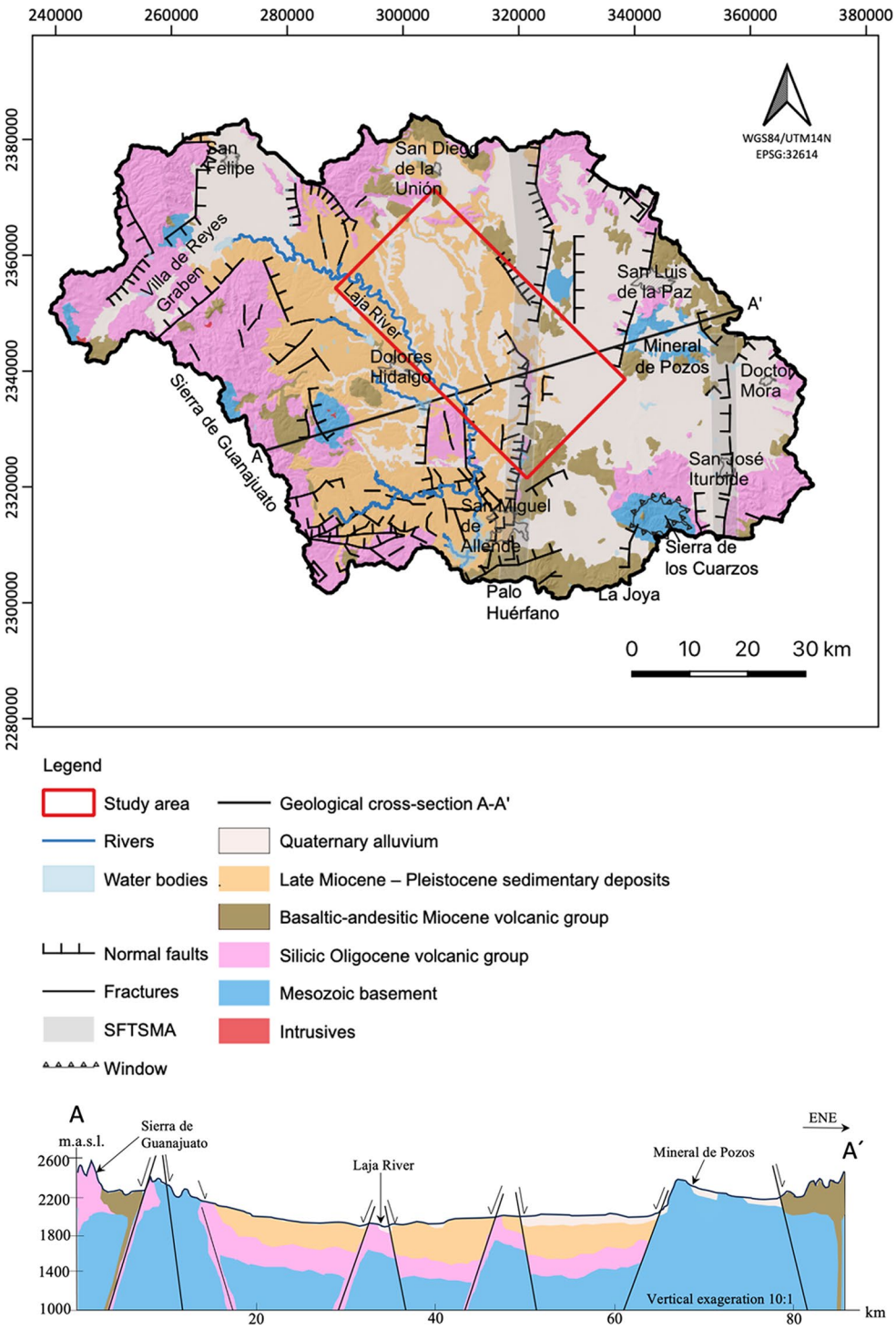

Fig. 3 CARL simplified geology. The cartography of the surface geology was synthesized from SGM (1997,1999). The structural geology was complemented with data from Alaniz-Álvarez et al. (2002, 2005) and Del Pilar-Martínez et al. (2020)

the Mesa Central physiographic province (INEGI 2001), where the N-S Taxco-San Miguel de Allende Fault System (SFTSMA) forms a cortical limit (Alaniz-Álvarez et al. 2001, 2002). The CARL stratigraphy can be described as follows:

Mesozoic basement

The Mesozoic basement is composed of Upper Jurassic to Cretaceous volcano-sedimentary, sedimentary and volcanic rocks. In the west, the volcano-sedimentary succession is exposed in the suture belt in Sierra de Guanajuato, formed by the closing and inversion of the Arperos basin during late Aptian (Martini et al. 2013, 2014). The Mesozoic rocks

are intruded by the Comanja Granite that crops out in the core of Sierra de Guanajuato with a reported crystallization age of 52.64±0.52 Ma and exhumation age of ~49 Ma (Olmos-Moya 2018). Volcano-sedimentary rocks crop out in the Sierra de los Cuarzos in the southern CARL (Martini et al. 2016), and the sedimentary calcareous unit outcrops in the footwall block of the San Miguel de Allende fault (Cid-Villegas et al. 2022). Cretaceous limestones and sandstones crop out to the east in Mineral de Pozos (Ortega-Flores at al. 2014).

Silicic oligocene volcanic group

This group includes rhyolitic domes, lava flows, pyroclastic deposits, and rhyolitic ignimbrites, volumetrically the most important part of the Oligocene volcanism, reaching 200 to 300 m of thickness in the study area (Nieto-Samaniego et al. 1999, 2005). During the Oligocene, extensional deformation was recorded through a complex system of normal N-S faults known as the Taxco – San Miguel de Allende Fault System (SFTSMA). Contemporary NE-SW and NW-SE normal faults and associated fractures were also active within the CARL (Alaniz-Álvarez et al. 2001). The synchrony between volcanism and fault activity during this time is represented by the alignment of the Chichíndaro rhyolite domes with N, NW and NE direction (Alaniz-Álvarez et al. 2002; Del Pilar-Martínez et al. 2020). The 30.82±0.52 Ma Duraznillo quartzmonzodioritic intrusive (Del Pilar-Martínez et al. 2020) is exposed south of the Villa de Reyes Graben (Fig. 3).

Basaltic-andesitic Miocene volcanic group

The silicic volcanism is unconformably overlain by Miocene basalts, andesites and trachyandesites that erupted through fissure eruptions within the basin and through the Palo Huérfano and La Joya stratovolcanoes (Nieto-Samaniego et al. 1999; Alaniz-Álvarez et al. 2002) at the south, forming the watershed of the basin. This volcanism is associated with the Miocene andesitic volcanic arc of the Trans-Mexican Volcanic Belt (Gómez-Tuena et al. 2005).

Late miocene – pleistocene sedimentary deposits

From late Miocene to the Pleistocene, the tectonic depressions were filled with continental sediments: gravels, sandstones and polymictic conglomerates poorly consolidated (Nieto-Samaniego et al. 1999, 2005; Alaniz-Álvarez et al. 2002) with thicknesses of around 400 m (Nieto-Samaniego et al.1999; CONAGUA 2020a, b). Lastly, a Quaternary alluvium was deposited.

Materials and methods

Seven thermal water samples (M-1, M-2, M-3, M-4, M-5, M-6, and M-7), with temperatures between 29 to 47ºC, were collected directly from discharge wells supplying spas (M-5 and M-6) and agricultural wells (M-1, M-2, M-3, M-4, and M-7) in November 2021 and November 2022. Physicochemical parameters were measured in situ. A temperature probe was used for the temperature measurements, a pHep® by Hanna for pH, a meter-hold for TDS and EC, ammonia and CO_2 were analyzed by a drop test SSQuim, Fe with an iron test kit by Hanna, and also paper test strips for the pH, alkalinity and chlorine. The samples were analyzed for anions, cations, silicon, trace elements, and stable isotopes (δD and $\delta^{18}O$) in the SLE laboratory of Earth Sciences of the CICESE in Baja California. The samples were collected in polypropylene containers and filtered with a cellulose nitrate membrane of 0.45 µm pore size. The samples to be analyzed for cations and trace elements were acidified with ultra-pure grade HNO_3 until reaching a pH less than 2. The following analytical techniques were used in the analysis of the water samples: cations and silicon by microwave plasma atomic emission spectrometry (MP-AES), anions by ion chromatography, trace elements by inductively coupled plasma mass spectroscopy (ICP-MS), and isotopes by laser spectroscopy.

Eighteen groundwater public wells (seven thermal and eleven non-thermal) with information of main ions, boron, arsenic, and temperature that were sampled during the rainy season (September-October) in 2020 were also analyzed. The information of the eighteen public wells was obtained from the Guanajuato State Water Commission (CEAG – by its initials in Spanish: Comisión Estatal de Aguas de Guanajuato) database through the National Transparency Portal.

The Piper and Stiff diagrams were made in R by using the USGS smwrGraphs package. The distribution of aqueous species and saturation indices of mineral phases were analyzed with the USGS PHREEQC Interactive v.3 software using the wateq4f thermodynamic database, and default pe = 4. Silica geothermometer was calculated with the spreadsheet by Powell and Cumming (2010). The iGeoT software (Reed and Spycher 1984; Spycher et al. 2016; Spycher and Finsterle 2016) was used to calculate the multicomponent geothermometers with a manually selected mineral assemblage, and PyGeoT processing tool to automate the mineral selection (Olguín-Martínez et al. 2022). The thermodynamic database was soltherm.h06 (Reed and Palandri 2006). A rock sample collected from the fault zone, close to sample M-3, was analyzed by X-ray diffraction (XRD) in the LICAMM laboratory of University of Guanajuato.

Results

Physico-chemical parameters and water classification

Sampling locations, the public wells from CEAG database, and their discharge temperature are shown in Fig. 4. Physico-chemical parameters and geochemical results for the seven samples collected in this study are listed in Table 1.

The discharge temperature of the thermal waters samples varied from 29ºC (M-6) to 47ºC (M-1), and the pH from 7.7 to 8. Magnesium value for sample M-7 is below the detection limit, and the value was estimated using the PyGeoT tool which calculates the optimized values of aluminum and magnesium through simulations developed in TOUGHREACT V3 (Xu et al. 2014). The charge balance error is within ±10% for the seven samples. The relative cation concentrations for all water samples are Na > Ca > Mg, and the relative anion concentrations are $HCO_3 > SO_4 > Cl$.

The dataset from the public wells (Table 2) taken during the rainy season (September and October) was used for comparison with the thermal water data due to proximity with the thermal water sampling date (November). The temperature of the public wells varies from 23 to 36ºC, of which seven are considered thermal water (more than 29ºC), and eleven are non-thermal.

The main ions of the seven thermal samples and the eighteen public wells were plotted on the Piper diagram (Fig. 5). The public wells were plotted using a color palette that goes from blue (23ºC) to red (36ºC). The waters are sodium-bicarbonate type, except three non-thermal samples (La Medina, Jesús María Chiquito, and San Gabriel) that are calcium-bicarbonate waters.

The major ion distribution in samples and public wells is shown as Stiff plots in Fig. 6. Bicarbonate is the main anion in all samples, and sodium is the dominant cation. However, calcium concentration increases east of the study area.

Fig. 7 shows the concentrations of the main constituents of the analyzed waters plotted on a Schoeller type plot (Truesdell 1991)

Geothermometry

The diagram Na-K-Mg, also known as geoindicators (Giggenbach 1988, 1991), is shown in Fig. 8. The waters plotted on the diagram were the ones with water sample

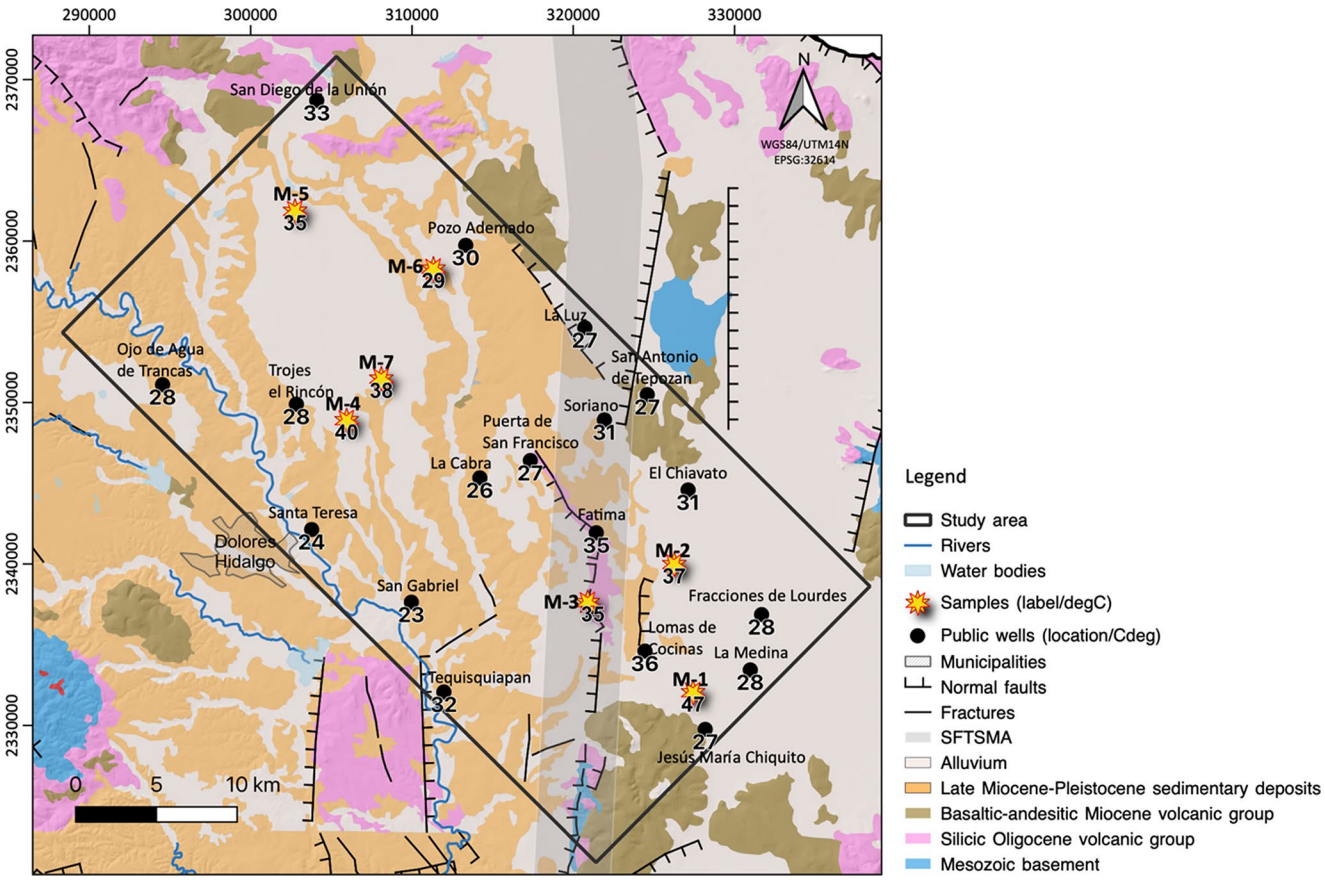

Fig. 4 Sampling locations. The public wells from the CEAG database are also displayed. Numbers indicate the discharge temperature in degrees Celsius. Samples and CEAG temperatures were taken during the rainy season

Table 1 Physico-chemical parameters, and concentrations of main ions, trace elements and stable isotopes for the seven water samples. Values below the detection limit are reported as bdl

Thermal sample	M-1	M-2	M-3	M-4	M-5	M-6	M-7
Date	03/11/21	03/11/21	03/11/21	03/11/21	16/11/22	16/11/22	16/11/22
T water (°C)	47	37	35	40	35	29	38
T air (°C)	25	26	24	26	19	19	19
pH	7.90	8.00	7.90	7.80	7.80	8.00	7.70
EC (µs/cm)	550.00	423.00	356.00	590.00	686.00	471.00	625.00
Na (mg/L)	82.88	58.18	50.29	102.71	109.95	45.30	107.97
K (mg/L)	10.20	15.18	14.28	11.89	8.43	8.45	4.91
Mg (mg/L)	2.00	2.66	3.34	1.48	1.13	1.88	bdl
Ca (mg/L)	31.08	32.68	35.25	33.93	18.62	32.82	30.82
SiO_2	72.46	93.66	94.07	90.71	73.36	97.90	63.01
Si (mg/L)	33.87	43.78	43.97	42.40	34.29	45.76	29.45
F (mg/L)	1.62	1.04	0.85	1.59	5.15	1.34	1.88
Cl (mg/L)	10.26	9.48	8.83	22.77	18.83	8.48	22.56
Br (mg/L)	bdl	bdl	bdl	bdl	bdl	bdl	bdl
NO_3 (mg/L)	bdl	bdl	bdl	bdl	5.95	6.58	7.08
SO_4 (mg/L)	8.83	10.06	10.58	11.89	20.75	23.45	49.55
HCO_3 (mg/L)	240.00	240.00	240.00	265.00	280.00	190.00	230.00
CO_2 (ppm)	8.00	7.80	7.80	7.60	7.60	7.40	7.40
Li (µg/L)	74.63	47.81	35.38	144.02	424.40	128.28	234.32
Rb (µg/L)	30.80	26.44	25.01	23.94	35.31	14.04	13.31
Cs (µg/L)	4.00	0.67	0.53	3.36	10.63	0.29	4.98
Sr (µg/L)	184.34	277.32	318.30	153.22	97.42	241.71	75.20
Ba (µg/L)	14.66	109.70	128.99	84.93	14.64	145.71	4.19
Cr (µg/L)	1.47	3.00	2.87	8.39	1.15	1.92	1.69
Mo (µg/L)	2.46	2.92	2.49	6.58	4.19	3.55	9.39
Mn (µg/L)	1.64	0.46	0.36	1.51	bdl	bdl	bdl
Fe (µg/L)	4.30	1.47	2.09	12.70	bdl	bdl	2.16
Co (µg/L)	<0.1	<0.1	<0.1	<0.1	<0.1	<0.1	<0.1
Ni (µg/L)	1.20	<1.0	<1.0	3.50	<1.0	<1.0	<1.0
Pb (µg/L)	<0.1	0.35	0.25	<0.1	<0.1	<0.1	<0.1
Cu (µg/L)	<1.1	<1.1	1.76	<1.1	<1.1	<1.1	<1.1
Zn (µg/L)	3.48	9.46	0.75	3.62	bdl	bdl	7.20
Cd (µg/L)	<0.1	<0.1	<0.1	<0.1	<0.1	<0.1	<0.1
B (µg/L)	198.35	105.44	90.12	278.54	418.72	142.40	281.36
Al (µg/L)	<4.0	<4.0	<4.0	<4.0	<4.0	<4.0	<4.0
Tl (µg/L)	<0.1	<0.1	<0.1	<0.1	<0.1	<0.1	<0.1
As (µg/L)	9.36	14.68	13.44	12.10	11.68	8.11	5.66
U (µg/L)	2.89	2.89	3.16	5.06	1.59	2.81	5.03
TDS (ppm)	276.00	213.00	188.00	570.00	324.00	230.00	327.00
$\delta^{18}O$ (‰)	-9.80	-10.29	-10.32	-8.94	-10.21	-10.82	-7.72
δD (‰)	-71.54	-74.29	-74.80	-66.74	-71.03	-75.54	-55.48
CBE (%)	9.8	3.3	1.6	9.6	0.8	-0.5	5.8

Table 2 Public wells data set

Well	T water (°C)	Na (mg/L)	K (mg/L)	Mg (mg/L)	Ca (mg/L)	F (mg/L)	Cl (mg/L)	HCO_3 (mg/L)	SO_4 (mg/L)	B (µg/L)	As (µg/L)
San Gabriel	23	75.26	16.19	4.69	62.70	0.10	21.71	360.53	62.19	86.20	11.70
Santa Teresa	24	67.29	10.54	2.50	17.15	0.67	13.63	245.53	7.47	240.40	14.20
La Cabra	26	76.15	23.39	4.83	33.30	0.85	21.78	253.77	55.33	214.10	27.20
Puerta de San Francisco	27	75.66	24.16	6.00	35.29	0.36	23.30	271.89	55.40	82.70	25.60
La Luz	27	81.73	17.48	4.88	31.32	0.10	28.78	279.72	47.68	201.80	25.60
San Antonio del Tepozan	27	84.97	18.05	4.36	36.61	0.10	27.58	258.68	47.42	0.27	28.30
Jesus Maria Chiquito	27	57.12	13.76	9.21	46.91	0.10	11.15	317.21	5.00	64.90	9.60
Ojo de Agua de Trancas	28	31.66	10.64	2.50	16.44	0.10	16.66	142.97	12.04	87.00	14.10
Trojes el Rincon	28	97.61	11.65	2.50	28.03	0.76	26.76	323.23	29.27	147.60	8.80
Fracciones de Lourdes	28	58.78	18.45	2.77	44.81	0.34	18.68	229.99	19.38	109.60	14.20
La Medina	28	29.53	13.04	3.50	61.24	0.10	11.22	247.73	13.87	56.20	8.50
Pozo Ademado	30	100.08	7.60	2.50	31.45	1.31	23.30	280.96	42.36	334.00	11.60
Soriano	31	75.78	13.68	3.14	28.89	0.10	26.76	292.15	39.95	185.30	24.40
El Chivato	31	90.54	30.04	2.50	28.66	0.25	20.20	254.86	27.77	180.90	17.40
Tequisquiapan	32	66.47	7.92	2.50	29.05	0.15	15.81	223.56	24.88	122.90	18.90
San Diego de la Union	33	71.19	18.21	5.54	25.83	0.31	19.25	235.64	39.38	79.80	9.50
Fatima	35	305.17	15.30	5.14	19.10	0.10	21.42	689.97	25.35	138.66	15.64
Loma de Cocinas	36	136.76	6.96	2.50	11.97	0.57	20.70	289.04	27.86	400.80	22.90

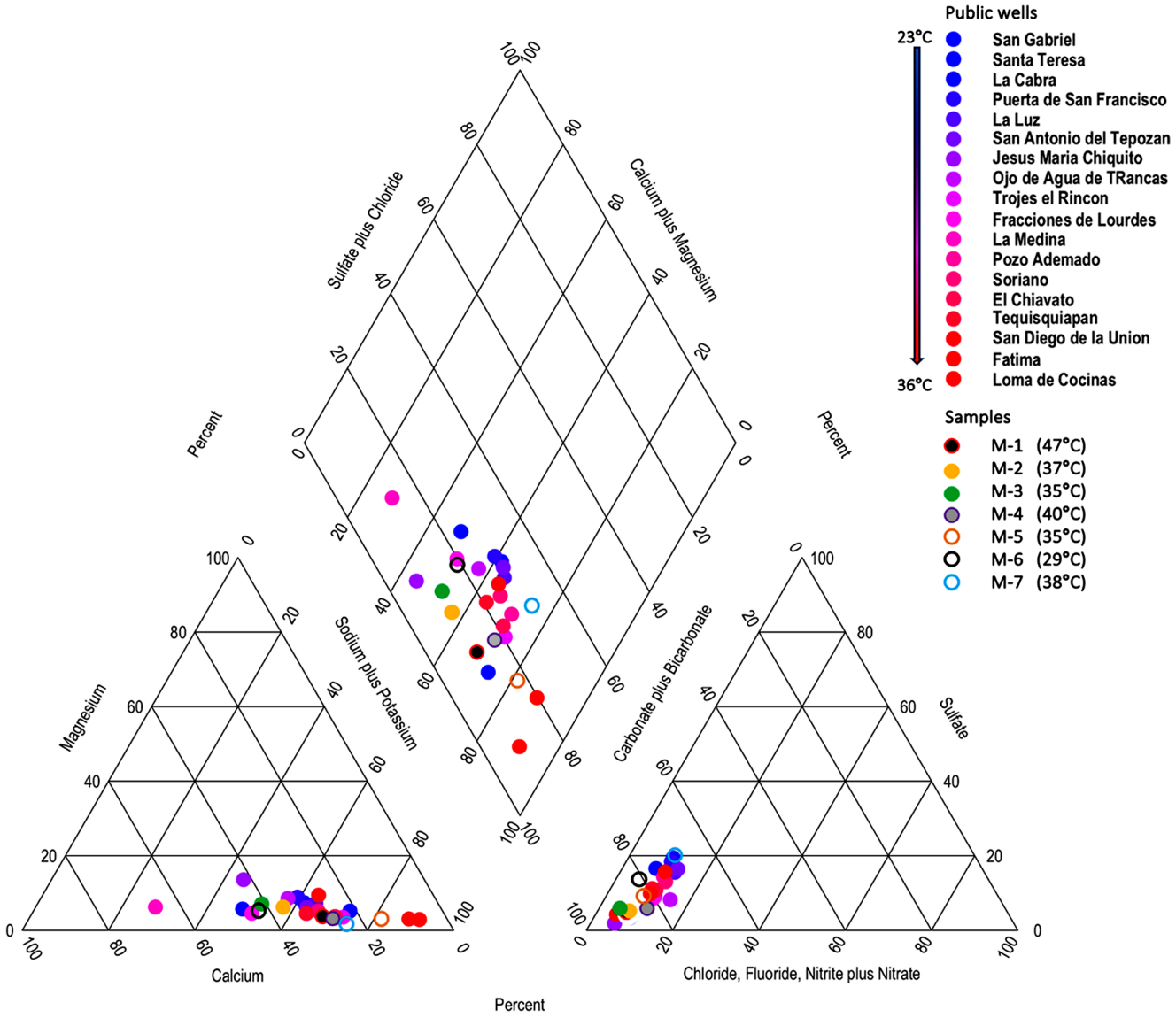

Fig. 5 Piper diagram for the seven samples and the eighteen public wells. The public wells were plotted using a color palette that goes from blue (23ºC) to red (36ºC). The palette used for the seven thermal samples is not related with their temperature

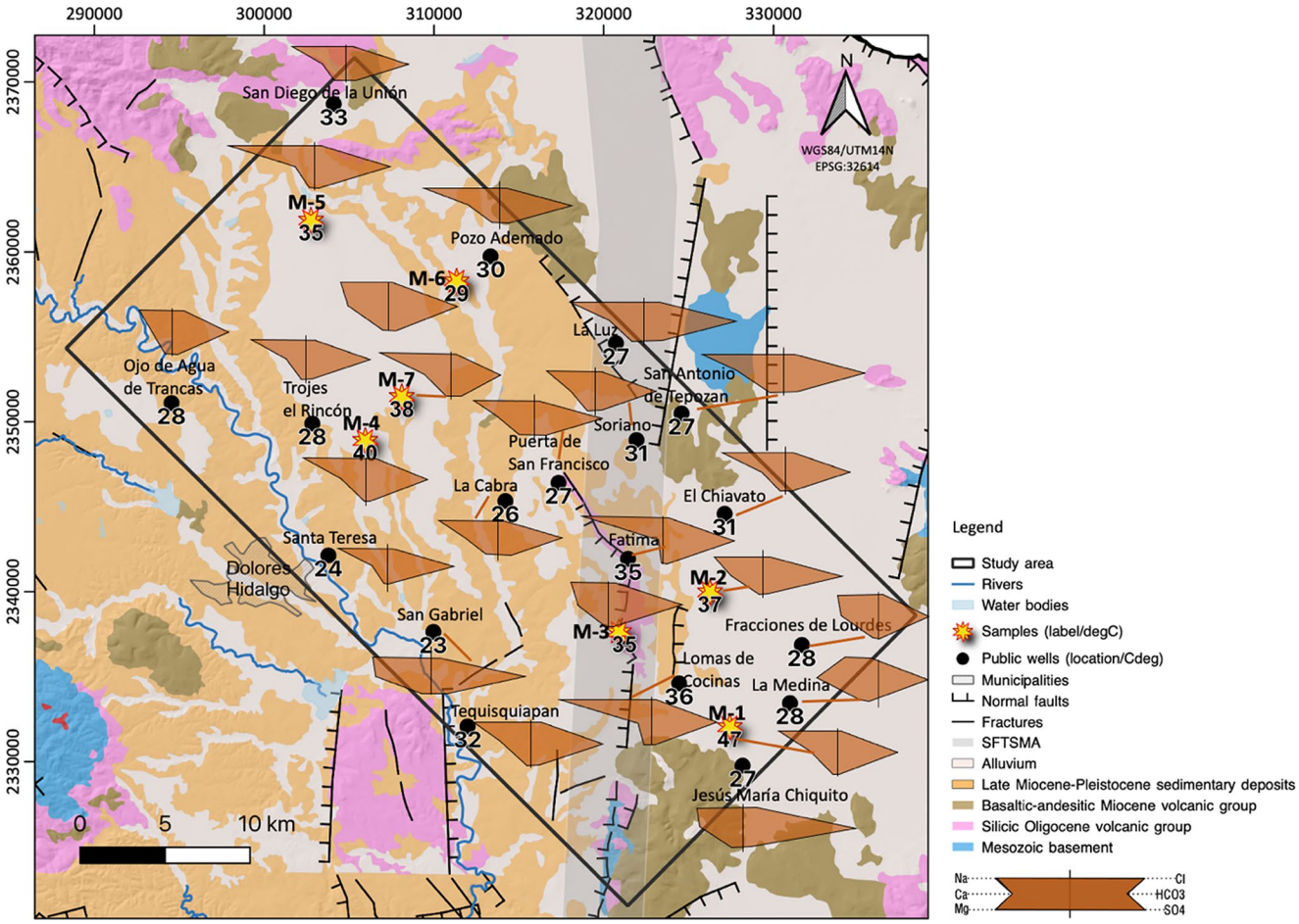

Fig. 6 Stiff plots of the seven samples and the eighteen public wells

label as M-1 to M-6. M-7 was not plotted because of its magnesium concentration value was under the detection limit. The six samples fall into the field of the immature waters; therefore, they do not comply with the thermodynamic conditions for the cation geothermometer application: Na-K, Na-K-Ca, and K-Mg (Fournier and Truesdell 1973; Giggenbach 1991).

As cation geothermometers cannot be applied to estimate the temperature at depth, other methodology can be applied: the multicomponent geothermometers (Cioni and Marini 2020). In order to understand how thermal waters interact with the rock-minerals, the equilibrium between the thermal waters and the surrounding mineral phases was investigated by analyzing the saturation indices of specific minerals at the most probable reservoir conditions, taking into account pH values and local geology. Only the saturation indices of the seven thermal-water samples were analyzed because they are the only ones with complete water analysis.

It is expected that under favorable conditions, the aqueous solution approaches and possibly attain the conditions of chemical equilibrium with host rocks with the generation of the final chemical composition of the water and the formation of hydrothermal alteration minerals (Cioni and Marini 2020). Multicomponent geothermometry is based on the saturation indices of selected minerals that are expected to occur in the reservoir over a wide range of temperatures. The selection of the mineral set was carried on manually and automatically. Manual mineral selection was based on the identified mineral assemblages present in the saturation indices calculated with PHREEQC. The saturation indices of the seven thermal samples at discharge temperature are shown in Fig. 9.

The automatic mineral selection was carried out statistically with the PyGeoT tool. Both, the manually and automatically selected minerals were used with the iGeoT program, where the temperature at which the final RMED value is at a minimum (T_{RMED}), the calculated value is then inferred to be the reservoir temperature. In the study area, silica is represented by chalcedony or amorphous silica (Mahlknecht et al. 2004), consequently, the chalcedony geothermometer (Fournier 1977) was also used, taking into consideration that the silica geothermometers are quite sensitive to dilution effects (Arnórsson 2000). The mineral saturation indices, log(Q/K), as function of temperature using the manual

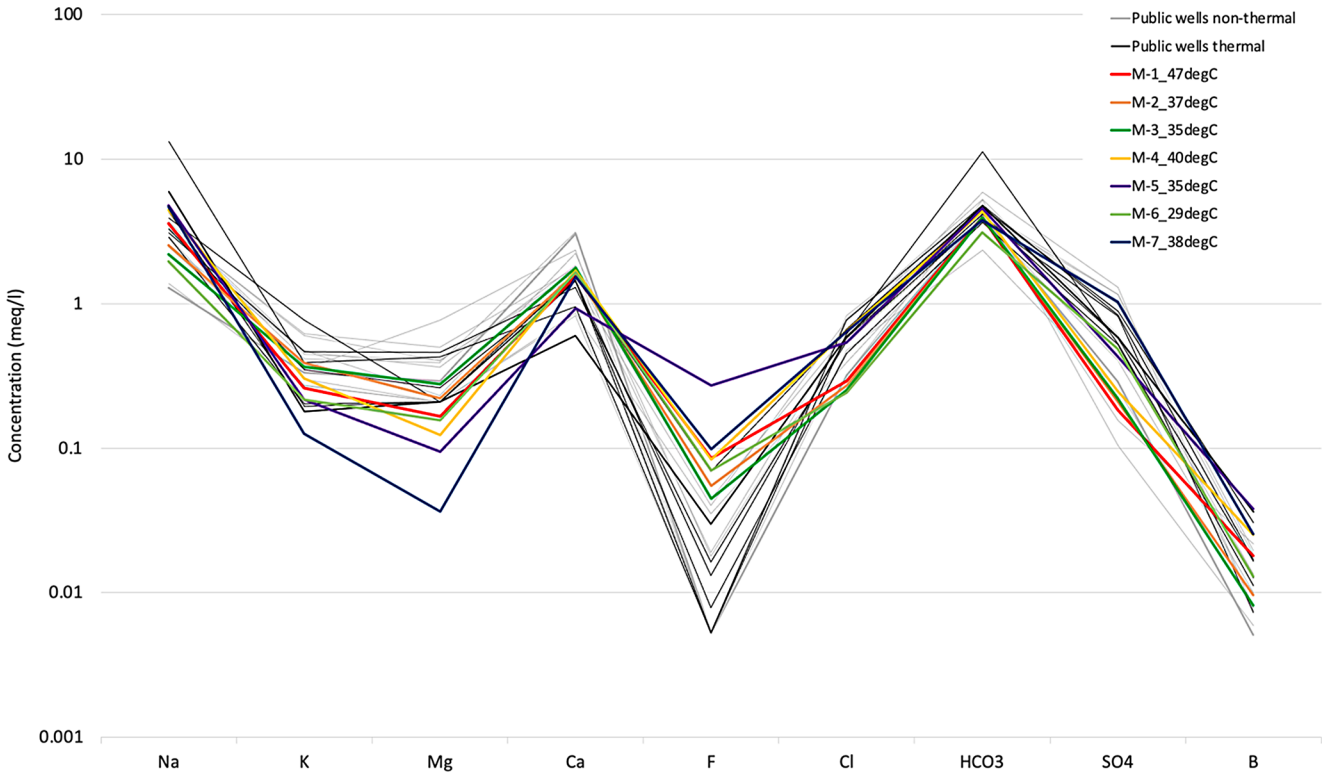

Fig. 7 Schoeller type plot (Truesdell 1991) showing the concentrations of the main constituents of the analyzed waters. The gray color is used for all the samples of non-thermal public wells and the black for the thermal public wells. The palette used for the thermal samples of this work is not related with their temperature

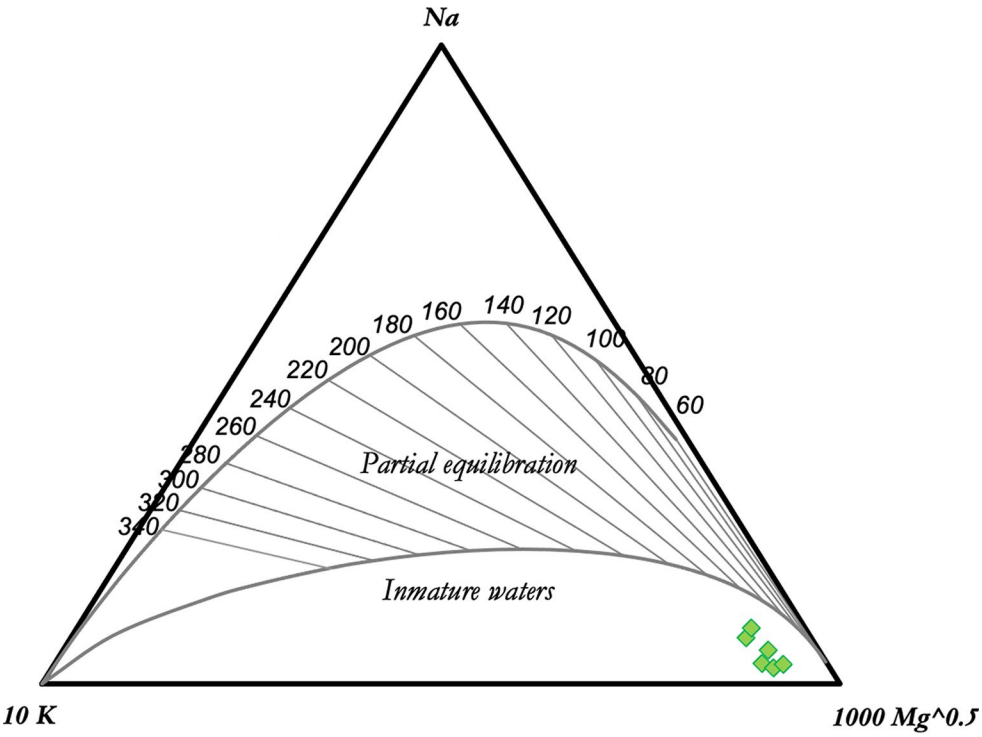

Fig. 8 Geoindicators Na-K-Mg (Giggenbach 1988, 1991). Six water samples: M-1 to M-6 plot in the immature water field

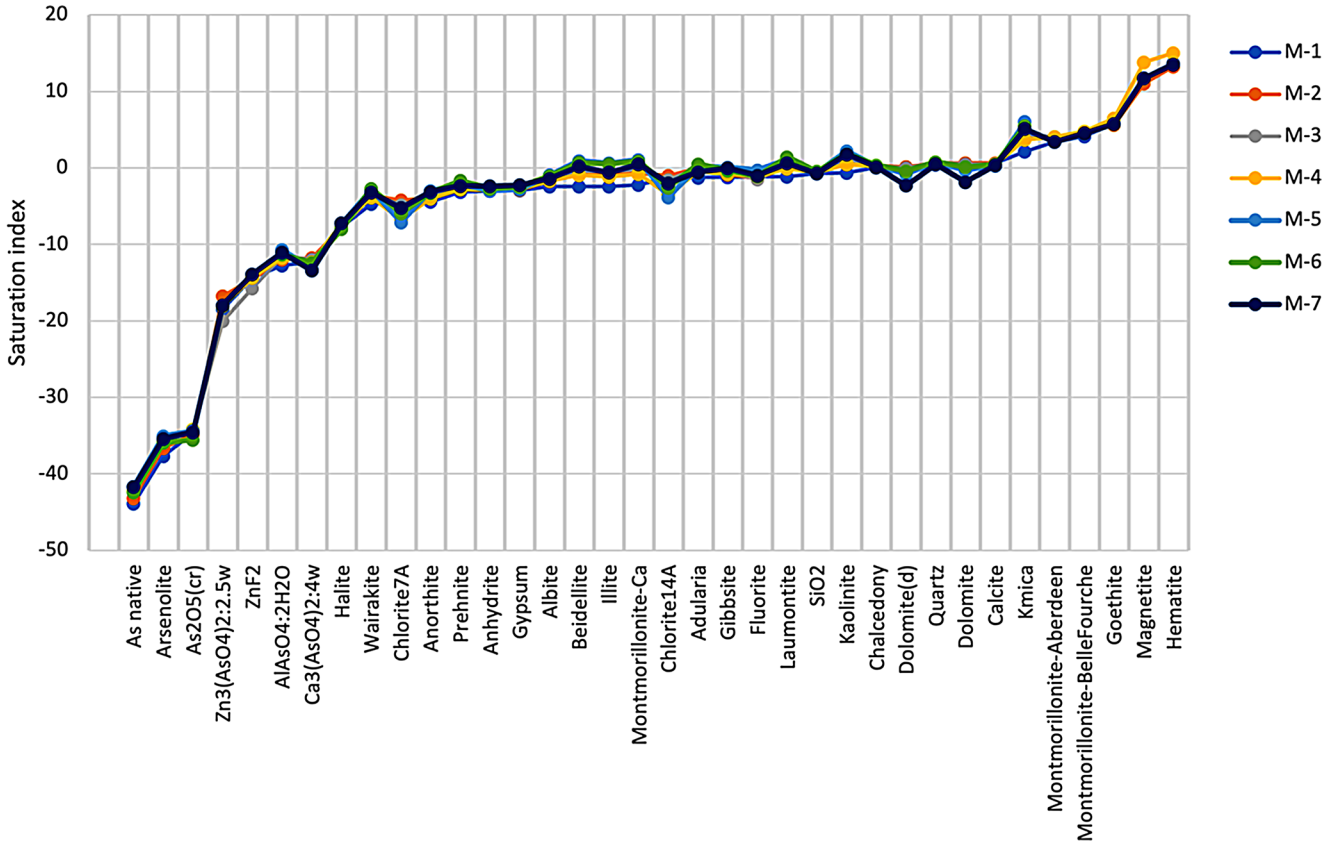

Fig. 9 Saturation indices of selected minerals for the seven thermal samples

mineral selection: chalcedony, laumontite, and montmorillonite are shown in Fig. 10. Table 3 lists the hydrothermal minerals of each sample chosen by PyGeoT more than ten times for the calculations. The calculated temperatures are listed on Table 4.

The temperatures calculated using multicomponent geothermometry yield values from 90 to 105 ºC. Chalcedony geothermometer indicates temperature values from 84 to 109ºC, while the temperatures calculated with PyGeoT are in the range from 100 to 126ºC. Reservoir temperatures can be classified as low-temperature geothermal waters (< 150ºC) (Barbier 2002).

Chloride and Boron distribution.

The Cl and B content of geothermal waters, and hence the Cl/B ratios, are widely used to distinguish reservoirs and to obtain information about the origin of the waters and other processes like mixing with groundwater, seawater, or magmatic fluids; generally, B and Cl show a linear trend indicating a common source (e.g. Arnórsson and Andrésdóttir 1995; Bernard et al. 2011; Morales-Arredondo et al. 2018; Hung-Chun et al. 2021).

Cl and B occur in volcanic rocks in trace amounts mainly as soluble salts on the primary minerals surfaces (Ellis and Mahon 1967). Cl is considered to be a conservative constituent, that means that, once added to the fluid phase, it remains there because it only forms soluble minerals (Arnórsson 2000). On the other hand, B acts as incompatible at high temperatures, but at low temperatures (below 100–150ºC), B is taken up from solution into secondary minerals (mainly illite), as well as into lake sediments, and organic soils (into clays, humus and peats) (Harder 1974).

The distribution of Cl and B in the thermal samples is shown in Fig. 11. It is observed a clear linear correlation in the concentrations of Cl and B in thermal samples M-1, M-2, M-3, M-5, and M-6; while thermal samples M-4 and M-7 diverge.

Stable isotopes ($\delta^{18}O$ and δD)

Stable isotopes ($\delta^{18}O$ and δD) are used for determination of the origin and processes that occur during thermal fluids ascend to the surface. Frequently, geothermal water presents an oxygen shift to more positive values; this $\delta^{18}O$ enrichment is caused by isotopic exchange with rock (Nicholson 1993; Drever 1997; Diamond 2022).

Stable isotopes of the seven thermal water samples are plotted in Fig. 12. The $\delta^{18}O$ values vary from − 10.8 to -7.7‰ whereas the δD varies from − 75.5 to -55.5‰. The

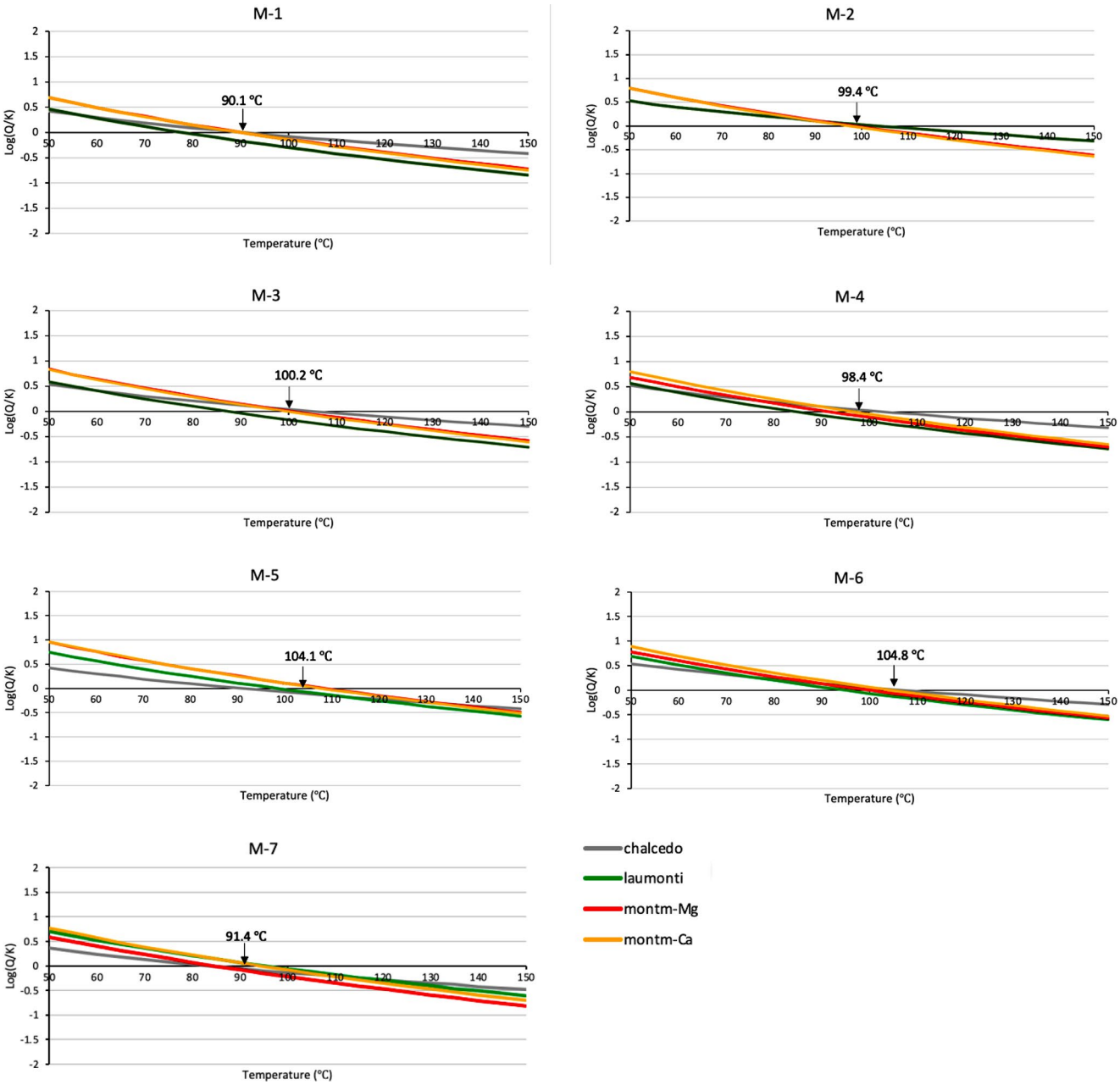

Fig. 10 Plots that represent the multicomponent geothermometry method using the seven thermal water samples. Computed saturation indices, log(Q/K), as a function of temperature. The reservoir temperature is inferred from the temperature at which RMED is minimum

Table 3 Hydrothermal minerals used in the PyGeoT tool. The number next to the name of the mineral is the number of times that the mineral is selected amongst the 20 best-clustering assemblages

M-1	M-2	M-3	M-4	M-5	M-6	M-7
paragonite (15)	kaolinite (16)	kaolinite (17)	kaolinite (17)	prehnite (17)	microcline (16)	prehnite (17)
chalcedony (14)	quartz (13)	microcline (12)	chalcedony (13)	quartz (16)	kaolinite (15)	quartz (16)
prehnite (14)	laumontite (13)	montm-Mg (11)	paragonite (12)	paragonite (13)	chalcedony (14)	laumontite (15)
laumontite (13)	clinozoisite (12)	quartz (11)	laumontite (12)	laumontite (13)	muscovite (12)	microcline (13)
montm-Mg (11)	microcline (12)	laumontite (11)	microcline (11)	microcline (12)	prehnite (12)	paragonite (12)
kaolinite (11)			montm-Mg (11)	kaolinite (12)	laumontite (12)	montm-Mg (11)
			prehnite (11)	montm-Mg (11)		kaolinite (11)

Table 4 Reservoir temperatures in ºC calculated with solute geothermometers

Geothermometer	M-1	M-2	M-3	M-4	M-5	M-6	M-7
Chalcedony	92	106	107	105	92	109	84
Multicomponent manual	90	99	100	98	104	105	91
Multicomponent PyGeoT	91	126	122	105	108	105	100

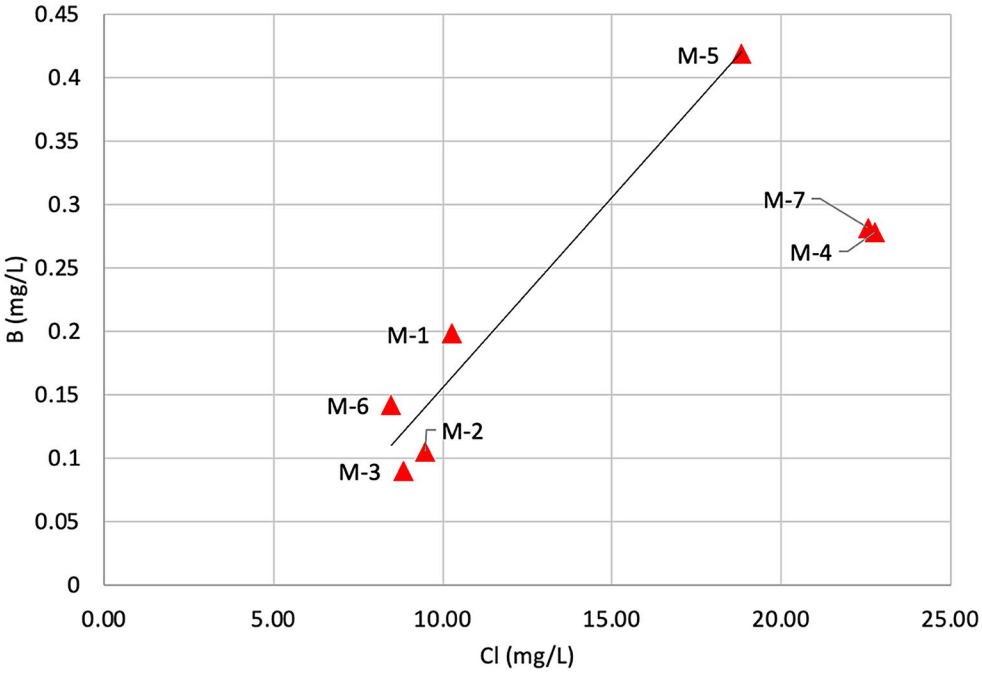

Fig. 11 Cl vs. B plot for the thermal samples collected in this work. A good linear correlation is obtained for the M-1, M-2, M-3, M-5, and M-6 samples with $R^2 = 0.94$

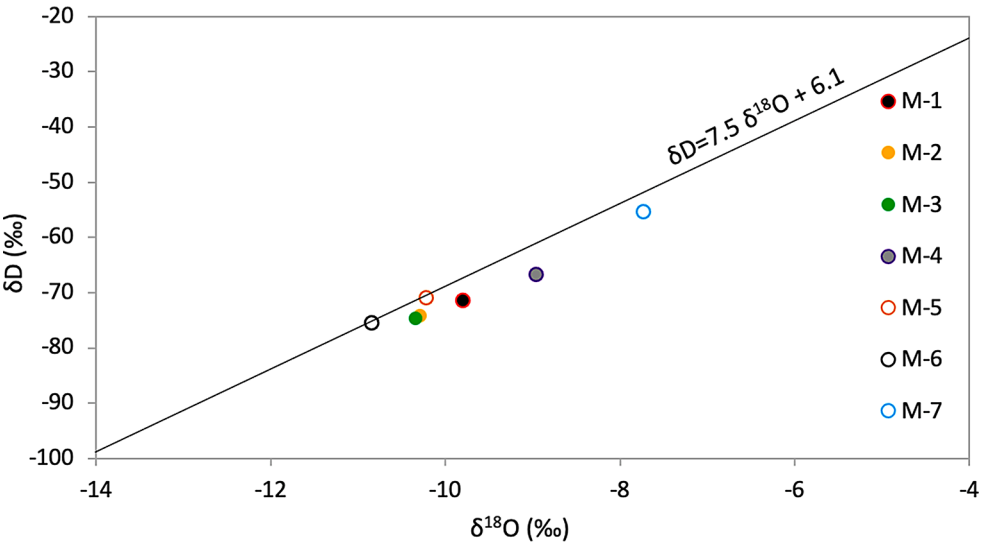

Fig. 12 Stable isotopes of the seven water samples. The regression for the Mexican precipitation line (Wassenaar et al. 2009) was used as regional meteoric water line

regression for the Mexican precipitation (Wassenaar et al. 2009) was used as regional meteoric water line. The thermal samples M-5 and M-6 plot on the meteoric water line, defined by $\delta D = 7.5\ \delta^{18}O + 6.1$, while the other samples (M-1, M-3, M-4, and M-7) plot slightly to the right, probably by evaporation effects. The oxygen shift is not evident in the isotopic composition of the thermal water, instead, a trend towards heavier isotope compositions of samples M-4 and M-7, which also differ from the rest of the samples in the Cl/B ratio.

Discussion

It is expected that thermal waters show enrichment in Na, K, F, Cl, and SO_4, while cold waters are enriched in Mg and Ca (Truesdell 1991). The analysis of the statistical descriptive

Schoeller plot does not provide evidence about the dominance of those elements, all waters samples show a very similar pattern. However, the thermal waters have a slight enrichment in fluoride (specially M-5), as also observed in other low-temperature systems in Guanajuato (Morales et al. 2015; Morales-Arredondo et al. 2016); while the non-thermal waters are slightly enriched in magnesium and calcium (especially on the wells located in the east). This geochemical behavior can be explained as a result of mixing of thermal waters with groundwater in the central part of the basin.

Chalcedony and multicomponent geothermometry suggest that at depth, the temperature may reach values between 84 and 126ºC. The mineral phases manually selected and used for multicomponent geothermometry were: chalcedony, montmorillonite, and laumontite. Those minerals were also selected more than ten times by the PyGeoT tool. Chalcedony and montmorillonite are reported by Mahlknecht et al. (2004) in the center of the basin. The occurrence of chalcedony, laumontite, and montmorillonite is a common alteration assemblage for a silicic rock type in low-temperature systems (Palmer et al. 2014). Temperature values from multicomponent geothermometry have to be taken carefully because of the poor reliability of aluminum concentrations of the seven water samples (all below the detection limit of 4 µg/L), and the absence of magnesium concentration from M-7. Typically, analyzed concentrations of magnesium from fluid samples collected from surface are higher than those obtained from deep wells, while the reverse is generally the case for aluminum (Olguín-Martínez et al. 2022). Aluminum concentration is very important in speciation-saturation calculations since most hydrothermal minerals are Al-silicates, thus, aluminum and magnesium concentrations strongly affect the computation of saturation indices (Spycher et al. 2014).

The characterization of the samples included the use of the Mifflin diagram (Mifflin 1968) that uses the hydrogeochemical indicators Na + K vs. Cl + SO_4 (in equivalents per million) to classify the water according to its evolution. The area closest to the origin, local flow, is associated with the recharge, while the higher concentrations are associated with higher evolution of the groundwater produced by a regional flow. Figure 13 shows that all analyzed waters (thermal and non-thermal) lie on the regional flow field.

The analysis of the Cl and B distribution shows that the samples located to the east of the study area present a good correlation, whereas the western samples M-4 and M-7 diverge. Thermal samples M-1, M-2, and M-3 are in the Laguna Seca aquifer, and samples M-4, M-5, M-6, and M-7 are in the Cuenca Alta del Río Laja aquifer. However, M-5 and M-6 display a similar Cl/B relationship with the thermal samples from Laguna Seca aquifer. This discrepancy may be related to an unreported fault that divides the eastern section where M-4 and M-7 samples are located. Buried geological faults have been considered before in the CARL (Piña-González et al. 2022).

In the study area, thermal and non-thermal waters have low chloride concentration, below 30 mg/L. Thermal water samples M-1, M-2, M-3, and M-6 have less chloride concentrations than non-thermal groundwater. Furthermore, M-4, M-5, and M-7 samples have more chloride than the thermal waters mentioned before, but still less chloride than the non-thermal waters from La Luz, San Antonio del Tepozan, and Trojes el Rincón. Mahlknecht et al. (2004) proposed that the high chloride content in shallow and intermediate-depth water (non-thermal groundwaters) could be agricultural related (irrigation return flow, and chloride rich fertilizers). Samples M-4, M-5, and M-7 (within the CARL aquifer) are located within an accelerated drawdown area with a high spatial density of pumping wells (Li et al. 2020); so, the chloride concentrations of those wells can be influenced by the agricultural activity, at the same time that the thermal component can be the result of an inverted cone of thermal water in transient state due to pumping (Ortega-Guerrero 2009).

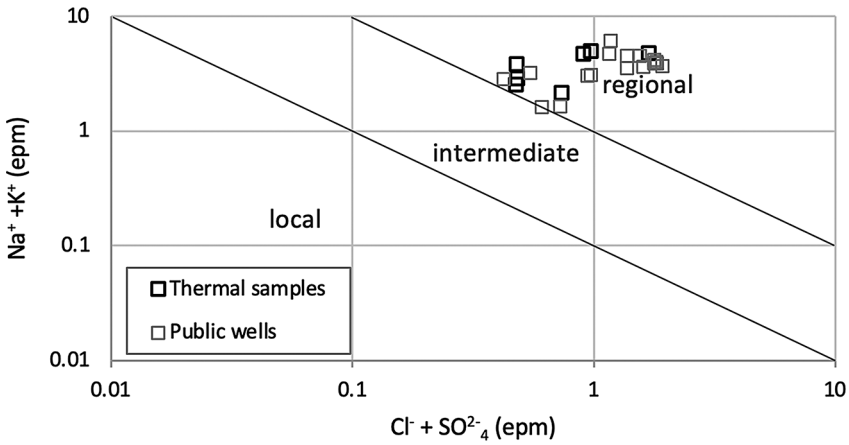

Fig. 13 Mifflin diagram for classification of the flow systems evolution. All analyzed waters lie on the regional flow field. Concentrations in equivalents per million

Regarding the relationship between faults and thermal water, in this study, M-1, M-2, and M-3 are closer to the SFTSMA fault zone. M-1 is the hottest water sample with 47ºC (4.5 km away from the fault trace), and M-3 (35ºC) is the one located on the fault trace. Rock sample collected close to site M-3 corresponds to a pyroclastic rock on the fault zone where hydrothermal alteration is evident. XRD analysis reports calcite (Fig. 14b) and it correlates with the slight calcium enrichment in M-3, contrasting with the adjacent public wells Fatima (35ºC) and Loma de Cocinas (36ºC) where sodium dominance is very clear. Calcite precipitation can promote the fracture-sealing process in the fault zone, lowering permeability. Nevertheless, Fatima and Loma de Cocinas are located at transfer zones, where normal fault-segments intersect. This transfer zones may enhance the permeability and channel the deep fluid circulation to the surface (Olvera-García et al. 2020).

Isotopic signatures ($\delta^{18}O$ and δD) of the seven samples of thermal water suggest a meteoric origin and the samples do not show the $\delta^{18}O$ shift that is frequently observed in geothermal waters. This may be interpreted as a predominance of groundwater at low temperature that hinders the isotopic exchange with the rocks as the isotopic composition of low-temperature groundwater typically resemble the isotopic composition of meteoric water (Diamond 2022). Samples M-4 and M-7 present heavier isotope compositions that might be related to evaporation effects or mixing with a different meteoric recharge.

Thermal and non-thermal waters show a regional flow system evolution according to the Mifflin diagram. Its evolution, lateral and vertical flow paths can be described as follows: Groundwater in the CARL is of meteoric origin, and most recharge comes from rainwater that infiltrates in the mountain ranges of Sierra de Santa Bárbara and Sierra de Guanajuato to the west of CARL, and in the Palo Huérfano and La Joya volcanoes in the south. Bicarbonate is generally the major anion for waters draining igneous and metamorphic rocks (Drever 1997), which agrees with the geological characteristics of the recharge zones. In the recharge zones, waters are predominantly calcium-bicarbonate type, and CO_2 gas dissolution and carbonate weathering are the predominant processes during the infiltration. In the discharge zones, waters are mainly sodium-bicarbonate, where the source of sodium is Na-bearing silicate minerals (albite) weathering (Mahlknecht et al. 2004). The preferential groundwater flow direction is towards the center of the basin, meaning longer flow paths and deeper circulation, where thermal and non-thermal waters have similar geochemical signatures. There is an slight calcium enrichment at the east of the SFTSMA, that is related to the dissolution of calcite from the Mesozoic limestones by the cold recharge water. In the center of the CARL, groundwater is hosted by a shallower granular aquifer and a deeper rhyolite/ignimbrite fractured aquifer (CONAGUA 2020a, b). Drilled wells in the center of the basin produce from the granular aquifer that corresponds to the 400 m of late Miocene-Pleistocene sedimentary deposits. It is suggested that the rising of deep thermal water is a combination of processes including groundwater pumping from the shallow-overexploited aquifers, and the vertical

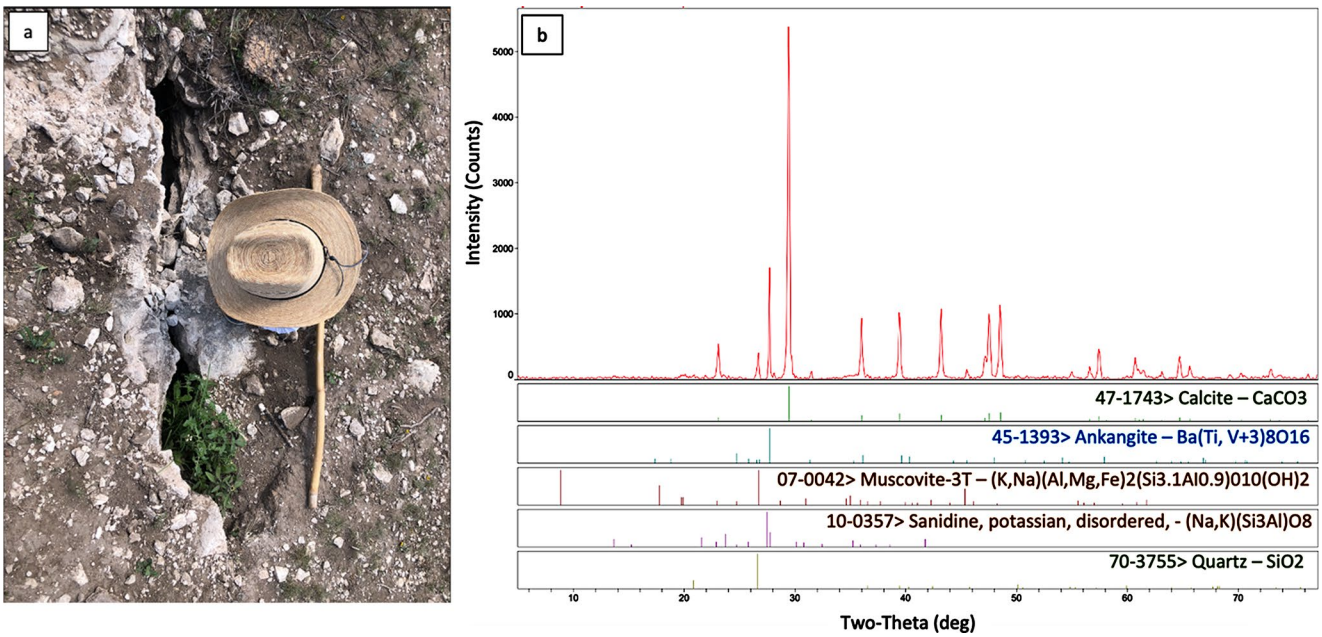

Fig. 14 Photograph of the hydrothermal alteration of pyroclastic rocks on the fault zone close to site M-3; **a**) outcrop where the rock sample was taken **b**) XRD analysis

permeability enhancement provided by the regional fault system SFTSMA (Axelsson 2008).

The overexploitation of the CARL is an eminent problem since groundwater is the only way to supply water to the population and the agricultural sector. Thermal waters are being used mainly for irrigation, increasing the risk of soil alkalinization (Besser et al. 2018). Nevertheless, the geothermal resource (from already operating wells) can also be used in the agriculture and agro-industry sectors as direct uses of geothermal energy, for example in aquaculture (fish farming and algae production). Deeper wells reaching the calculated reservoir temperature (~100ºC), could be used in food processing, fruit wine making, milk evaporation, and fruit, vegetables and grains drying, which could add an aggregated value to the agricultural production.

Conclusions

The thermal waters in the center of the CARL are sodium-bicarbonate type with similar geochemical signatures than the non-thermal waters, showing a regional flow system evolution. Temperature at depth was calculated using multicomponent geothermometry that indicates a range from 90 to 126ºC, while chalcedony geothermometer yields values between 84 and 109ºC. Isotopic composition ($\delta^{18}O$ and δD) of thermal water suggest a meteoric origin without $\delta^{18}O$ enrichment related with the low temperature. The Cl and B concentration in the thermal waters provides evidence for the presence of a barrier that detaches the central-western zone from the rest of the samples in the Laguna Seca and Cuenca Alta del Río Laja aquifers.

Author contributions

Lucía Magali Ramírez-González: Conceptualization, Methodology, Formal analysis and Investigation, Writing-original draft preparation, Visualization. María Jesús Puy Y Alquiza: Conceptualization, Methodology, Investigation, Resources, Writing – review and editing, Supervision, Funding acquisition. Yanmei Li: Conceptualization, Methodology, Investigation, Supervision, Funding acquisition. J. Horacio Hernández-Anguiano: Conceptualization, Methodology, Investigation, Supervision, Funding acquisition. Raúl Miranda-Avilés: Conceptualization, Supervision. Rosa María Prol-Ledesma: Conceptualization, Investigation, Writing – review and editing, Supervision.

Acknowledgements This research was financed by the Institutional Convening for Scientific Research (CIIC)-2022, Modality I, from the University of Guanajuato. We appreciate the support from Jesús René Báez Espinoza and Omar Vargas Rodríguez during the field work. We are very grateful to the water-well owners for allowing us to take the water samples: Iker Iñarritu, Juan Pablo Iñarritu, Rubén López, Mr. Alfredo, Martín García, José Villegas, and Pablo Rendón. We are also thankful to the Guanajuato State Water Commission (CEAG) for sharing the public wells information from its database. This study is part of the first author Ph.D. research, founded by the Mexican entity National Council of Humanities Science and Technology (CONAHCYT), doctoral scholarship with CVU 676194.

Data availability The data sets analyzed during the current study are included in the tables of the manuscript. Any other information is available from the corresponding author on reasonable request.

Declarations

Competing interests The authors declare that they have no known competing financial interests of personal relationships that could have appeared to influence the work reported in this paper.

References

Alaniz-Álvarez SA, Nieto-Samaniego ÁF (2005) El sistema de fallas Taxco-San Miguel de Allende y la Faja Volcánica Transmexicana, dos fronteras tectónicas del centro de México activas durante el Cenozoico. Boletín de la Sociedad Geológica Mexicana, Volumen conmemorativo del centenario grandes fronteras tectónicas de México, Tomo LVII, Núm. 1, 2005, pp. 65–82

Alaniz-Álvarez SA, Nieto-Samaniego AF, Reyes-Zaragoza MA, Orozco-Esquivel MT, Ojeda- García AC, Vassallo LF (2001) Estratigrafía Y deformación extensional en la región San Miguel De Allende-Querétaro, vol 18. Revista Mexicana de Ciencias Geológicas, México, pp 129–148

Alaniz-Álvarez SA, Nieto-Samaniego AF, Orozco-Esquivel MT, Vasallo LF, Xu S (2002) El sistema de fallas Taxco-San Miguel de Allende: Implicaciones de la deformación post-eocénica del centro de México. Boletín de la Sociedad Geológica Mexicana, Tomo LV, Núm. 1, 2002. P. 12–29

Arnórsson S (2000) Isotopic and chemical techniques in geothermal exploration development and use: sampling methods, data handling, interpretation. International Atomic Energy Agency, Vienna, p 351

Arnórsson S, Andrésdóttir A (1995) Processes controlling the distribution of boron and chlorine in natural waters in Iceland. Geochim Cosmochim Acta 59(20):4125–4146 0016-7037(95)00278-2

Axelsson G (2008) Production capacity of geothermal systems. Proceedings of the Workshop for Decision Makers on the Direct Heating Use of Geothermal Resources in Asia, Tianjin, China. 14 pp

Barbier E (2002) Geothermal energy technology and current status: an overview. Renew Sustain Energy Rev 6:3–65

Bernard R, Taran Y, Pennisi M, Tello E, Ramirez A (2011) Chloride and Boron behavior in fluids of Los Humeros geothermal field (Mexico): a model based on the existence of deep acid brine. Appl Geochem 26:2064–2073. https://doi.org/10.1016/j.apgeochem.2011.07.004

Besser H, Mokadem N, Redhaounia B, Hadji R, Hamad A, Hamed Y (2018) Groundwater mixing and geochemical assessment of low-enthalpy resources in the geothermal field of southwestern Tunisia. Euro-Mediterranean Journal for Environmental Integration (2018) 3:16. https://doi.org/10.1007/s41207-018-0055-z

Ch H-C, Ju-Lien P, Chen-Feng Y, Ying-Tzung S, Hsueh-Yu L, Kuo-Fang H, Hou-Chun L, Chuan-Hsiung C (2021) Hydrogeology constrained by multi-isotopes and volatiles geochemistry of Hot

Springs in Tatun Volcanic Group, Taiwan. J Hydrol 600:126515. https://doi.org/10.1016/j.jhydrol.2021.126515
Cid-Villegas G, Alaniz-Álvarez SA, Xu S, Vázquez-Serrano A, Juárez-Arriaga E (2022) Deformación Del Cretácico tardío en El límite de la Mesa Central Y La Sierra Madre Oriental, centro México. Boletín De La Sociedad Geológica Mexicana 74(2):A230222
Cioni R, Marini L (2020) A Thermodynamic Approach to Water Geothermometry. Springer Geochemistry. ISBN 978-3-030-54318-1 (eBook)
CONAGUA (2020d) Actualización de la disponibilidad media anual de agua en el acuífero Dr.Mora-San José Iturbide (1106) Estado de Guanajuato. Reporte de la subdirección General Técnica, Gerencia de Aguas Subterráneas. Ciudad de México, Diciembre 2020
CONAGUA (2020e) Actualización de la disponibilidad media anual de agua en el acuífero Santa María del Río (2417) Estado de Guanajuato. Reporte de la subdirección General Técnica, Gerencia de Aguas Subterráneas. Ciudad de México, Diciembre 2020
CONAGUA (2020a) Actualización de la disponibilidad media anual de agua en el acuífero Cuenca Alta del Río Laja (1108) Estado de Guanajuato. Reporte de la subdirección General Técnica, Gerencia de Aguas Subterráneas. Ciudad de México, Diciembre 2020
CONAGUA (2020b) Actualización de la disponibilidad media anual de agua en el acuífero Laguna Seca (1104) Estado de Guanajuato. Reporte de la subdirección General Técnica, Gerencia de Aguas Subterráneas. Ciudad de México, Diciembre 2020
CONAGUA (2020c) Actualización de la disponibilidad media anual de agua en el acuífero San Miguel de Allende (1107) Estado de Guanajuato. Reporte de la subdirección General Técnica, Gerencia de Aguas Subterráneas. Ciudad de México, Diciembre 2020
Custodio E, Llamas MR (1983) Hidrología Subterránea, Segunda Edición, Tomo 1. Omega. ISBN 84-282-0447-0
Del Pilar-Martínez A, Nieto-Samaniego AF, Alaniz-Alvarez S (2020) Development of a brittle Triaxial Deformation Zone in the Upper Crust: the case of the Southern Mesa Central of Mexico. Tectonics 39. https://doi.org/10.1029/2020TC006166
Diamond RE (2022) Stable Isotope Hydrology. The Groundwater Project, Guelph, Ontario, Canada. https://doi.org/10.21083/978-1-77470-043-3
Drever IJ (1997) The Geochemistry of Natural Waters, Surface and Groundwater Environments. Third Edition. ISBN 0-13-272790-0. 436 p
Ellis AJ, Mahon WAJ (1967) Natural hydrothermal systems and experimental hot water/rock interactions, part 1. Geochim Cosmochim Acta 31:519–538
Fitz-Díaz E, Lawton T, Juárez-Arriaga E, Chávez-Cabello G (2018) The cretaceous-paleogene Mexican orogen: structure, basin developmen, magmatism and tectonics. Earth Sci Rev 183:56–84
Fournier RO (1977) Chemical geothermometers and mixing models for geothermal systems. Geothermics 5(1–4):41–50
Fournier RO, Truesdell AH (1973) An empirical Na-K-Ca geothermometer for natural waters. Geochim Cosmochim Acta 37(5):1255–1275
Giggenbach WF (1988) Geothermal solute equilibria. Derivation of Na-K-Mg-Ca geoindicators. Geochim Cosmochim Acta 52(12):2749–2765
Giggenbach WF (1991) Chemical techniques in geothermal exploration, in UNITAR/UNDP Guidebook: Application of geochemistry in resources development, 119–144
Gómez-Tuena A, Orozco-Esquivel MT, Ferrari L (2005) Petrogénesis ígnea de la Faja Volcánica Transmexicana. Boletín de la Sociedad Geológica Mexicana. Volumen conmemorativo del Centenario. Tomo LVII, núm., 3, pp. 227–283
Harder H (1974) Boron. In handbook of Geochemistry. Springer-, pp. B-O
INEGI (2019) Zona Hidrogeológica Alta Río Laja Serie II, Escala 1:250,000. Conjunto De Datos. Accessed 13/10/2023: https://www.inegi.org.mx/app/biblioteca/ficha.html?upc=889463769200
INEGI (2021) Continuo De Elevaciones Mexicano. Accessed 13/10/2023: https://www.inegi.org.mx/app/geo2/elevacionesmex/
INEGI (1998) Estudio hidrológico del Estado de Guanajuato. ISBN 970-13-1916-8
INEGI (2001) Conjunto de Datos Vectoriales Fisiográficos (Physiographic vector data set.). Scale 1:1´000,000. Serie I
Knappett PSK, Li Y, Loza I, Hernandez H, Avilés M, Haaf D, Majumder S, Huang Y, Lynch B, Piña V, Wang J, Winkel L, Mahlknecht J, Datta S, Thurston W, Terrell D, Nordstrom DK (2020) Rising arsenic concentrations from dewatering a geothermally influenced aquifer in central Mexico. Water Res J 185(2020):116557–116516. https://doi.org/10.1016/j.watres.2020.116257
Li Y, Hernández H, Aviles M, Knappett PSK, Giardino JR, Miranda R, Puy MJ, Padilla F, Morales J (2020) Empirical bayesian kriging method to evaluate inter-annual wáter-table evolution in the Cuenca Alta Del Río Laja aquifer, Guanajuato, Mexico. J Hydrol 582(2020):124517. https://doi.org/10.1016/j.jhydrol.2019.124517
Mahlknecht J, Schneider JF, Merkel BJ, Navarro-de-León I, Bernasconi SM (2004) Groundwater recharge in a sedimentary basin in semi-arid Mexico. Hydrogeol J 12:511–530. https://doi.org/10.1007/s10040-004-0332-6
Martini M, Solari L, Camprubí A (2013) Kinematics of the Gurerrero terrain accretion in the Sierra De Guanajuato, central Mexico: new insights for the structural evolution arc-continent collisional zones. Int Geol Rev 55(5):574–589. https://doi.org/10.1080/00206814.2012.729361
Martini M, Solari L, López-Martínez M (2014) Correlating the Arperos Basin from Guanajuato, central Mexico, to Santo Tomás, southern Mexico: Implications for the paleogeography and origin of the Gurerreo terrane. Geosphere, v. 10; No. 6
Martini M, Solé J, Garduño-Martínez DE, Pi Puig T, Omaña L (2016) Evidence for two cretaceous superposed orogenic belts in Central Mexico based on paleontologic and K-Ar geochronologic data from the Sierra De Los Cuarzos. Geosphere 12:1–14
Mifflin MD (1968) Delineation of Ground-Water Flow Systems in Nevada. Doctoral dissertation, University of Nevada, Reno
Morales I, Villanueva-Estrada RE, Rodríguez R, Armienta MA (2015) Geological, hydrogeological, and geotermal factors associated to the origin of arsenic, fluoride, and groundwater temperature in a volcanic environment El Bajío Guanajuatense, Mexico. Environ Earth Sci 74:5403–5415. https://doi.org/10.1007/s12665-015-4554-9
Morales-Arredondo I, Rodríguez R, Armienta MA, Villanueva-Estrada RE (2016) The origin of groundwater arsenic and fluoride in a volcanic sedimentary basin in central Mexico: a hydrochemistry hypothesis. Hydrogeol J. https://doi.org/10.1007/s10040-015-1357-8
Morales-Arredondo JI, Esteller-Alberich MV, Armienta-Hernández MA, Martínez-Florentino TAK (2018) Characterizing the hydrogeochemistry of two low-temperature termal systems in Central Mexico. J Geochem Explor 185:93–104. https://doi.org/10.1016/j.gexplo.2017.11.006
Navarro de León I, Gárfias-Soliz J, Mahlknecht J (2005) Groundwater flow regime under natural conditions as inferred from past evidence and contemporary field observations in a semi-arid basin: Cuenca De La Independencia, Guanajuato, Mexico. J Arid Environ 63:756–771. https://doi.org/10.1016/j.jaridenv.2005.04.003
Nguyen MV, Arason S, Gissurason M, Pálson PG (2015) Uses of geothermal energy in food and agriculture. Opportunities for developing countries. FAO, Rome

Nicholson K (1993) Geothermal fluids. Chemistry and Exploration techniques. Springer-

Nieto-Samaniego ÁF, Ferrari L, Alaniz-Alvarez SA, Labarthe-Hernández G, Rosas-Elguera J (1999) Variations of cenozoic extensión and volcanism across the southern Sierra Madre Occidental volcanic province, Mexico, vol 111. GSA Bulletin, pp 347–363. no. 3

Nieto-Samaniego ÁF, Alaniz-Álvarez SA, Camprubí A (2005) La Mesa Central De México: estratigrafía, estructura y evolución tectónica cenozoica. Boletín De La Sociedad Geológica Mexicana Tomo LVII(N–m 3):285–318

NOM-127-SSA1-2021 NORMA Oficial Mexicana NOM-127-SSA1-2021 Agua para uso y consumo humano. Límites permisibles de la calidad del agua. DOF – Diario Oficial de la Federación: 02/05/2022

Olguín-Martínez MG, Peiffer L, Dobson PF, Spycher N, Inguaggiato C, Wanner C, Hoyos A, Wurl J, Makovsky K, Ruiz-Aguilar D (2022) PyGeoT: a tool to automate mineral selection for multicomponent geothermometry. Geothermics 104:102467

Olmos-Moya MJP (2018) Exhumación de los intrusivos Comanja y Tesorera: Implicaciones en el levantamiento de la Mesa Central de México. Tesis de Maestría. Universidad Nacional Autónoma de México. Recuperado de: https://repositorio.uanm.mx/contenidos/3503239

Olvera-García E, Garduño-Monroy VH, Liotta D, Brogi A, Bermejo-Santoyo G, Guevara-Alday JA (2020) Neogene-Quaternary normal and transfer faults controlling Deep-seated geothermal systems: The case of San Agustín del Maíz (central Trans-Mexican Volcanic Belt, México). Geothermics 86 (2020) 101791. https://doi.org/10.1016/j.geothermics.2019.101791

Ortega-Flores B, Solari L, Lawton TF, Ortega-Obregón C (2014) Detrital-zircon record of major middle triassic-early cretaceous provenance shift, central Mexico: demise of Gondwanan continental fluvial systems and onset of back-arc volcanism and sedimentation. Int Geol Rev 56(2):237–261

Ortega-Guerrero MA (2009) Presencia, distribución, hidrogeoquímica y origen de arsénico, fluoruro y otros elementos traza disueltos en agua subterránea, a escala de cuenca hidrológica tributaria de Lerma- Chapala, México. Revista Mexicana de Ciencias Geológicas, Vol.26, núm. 1, 2009, p, 143–161

Palmer CD, Ohly SR, Smith RW, Neuoane G, McLing T, Mattson E (2014) Mineral Selection for Multicomponent Equilibrium Geothermometry. GRC Transactions, Vol. 38, 2014

Panichi C, La Ruffa G (2009) Thermal springs. In: Silveira L, Usunoff E (eds) Encyclopedia of Life Support systems (EOLSS). Groundwater – volume I. Eolss Publishers Co. Ltd., Oxford, UK, pp 326–349

Piña-González V, Miranda-Avilés R, Hernández-Anguiano JH, Knappett PSK, Morales-Martínez JL, Puy-Alquiza MJ, Naves A, Bian J, Liu J, Ramírez-González LM, Navarro-Céspedes JM, Li Y (2022) Influence of geological faults on disolved arsenic concentrations in an overexploited aquifer with shallow geothermal heat. Applied Geochemistry 144(2022) 105395. https://doi.org/10.1016/j.apgeochem.2022.105395

Popovski K, Vasileyska SP (2004) Direct application of geothermal energy. Chapter 7:114–149

Powell T, Cumming W (2010) Spreadsheets for geothermal water and gas geochemistry. Proceedings, 35th Workshop on Geothermal Reservoir Engineering, Stanford University, California, February 1–3, 2010. SGP-TR-188

Reed M, Palandri J (2006) SOLTHERM. H06, a database of equilibrium constants for minerals and aqueous species. Available from the authors

Reed MH, Spycher N (1984) Calculation of pH and Mineral Equilibria in Hydrothermal Waters with application to Geothermometry and studies of Boiling and Dilution. Geochemica et Cosmochim Acta (48), 1479–1492

Salamanca-Corredor MA, Puy-Alquiza MJ (2017) Jóvenes en la Ciencia 2(1):1589–1593. https://www.jovenesenlaciencia.ugto.mx/index.php/jovenesenlaciencia/article/view/1354 Caracterización hidrogeoquímica de las fuentes de aguas termales del corredor San Miguel de Allende-Atotonilco

Servicio Metereológico Nacional Climatic Data Guanajuato. Accessed 13/10/2023: https://smn.conagua.gob.mx/es/informacion-climatologica-por-estado?estado=gto

SGM (Servicio Geológico Mexicano) (1997) Carta geológica-minera Guanajuato F14-7

SGM (Servicio Geológico Mexicano) (1999) Carta geológica-minera Querétaro F14-10

Spycher N, Finsterle S (2016) iGeoT v1.0: automatic parameter estimation for Multicomponent Geothermometry, user's guide. LBNL-1005841

Spycher N, Peiffer L, Sonnenthal EL, Saldi G, Reed MH, Kennedy BM (2014) Integrated multicomponent solute geothermometry. Geothermics 51:113–123

Spycher N, Peiffer L, Finsterle S (2016) GeoT user's Guide, A Computer Program for Multicomponent Geothermometry and Geochemical Speciation, Version 2.1. LBNL Report

Truesdell A (1991) Effects of physical processes on geothermal fluids. In: D'Amore F (coordinator) (ed) Applications of Geochemistry in Geothermal Reservoir Development. UNITAR/UNDP, Rome, pp 71–92

Wassenaar LI, Van Wilgenburg SL, Larson K, Hobson KA (2009) A groundwater isoscape (δD, δ18O) for Mexico. J Geochem Explor 102:123–136

World Health Organization (2022) Guidelines for drinking-water quality: fourth edition incorporating the first and second addenda. ISBN 978-92-4-004506-4 (electronic version)

Xu T, Sonnenthal EL, Spycher N, Zheng L (2014) TOUGHREACT V3.0-OMP Reference Manual: A Parallel Simulation Program for Non-Isothermal Multiphase Geochemical Reactive Transport. LBNL Manual. http://esdl.lbl.gov/FILES/research/